Applied Thermal Engineering 255 (2024) 123977

Contents lists available at ScienceDirect

Applied Thermal Engineering

journal homepage: www.elsevier.com/locate/apthermeng

Research Paper

Continuously stirred tank reactor for oil-suspended thermochemical energy storage systems for $CuSO_4{\cdot}5H_2O$

G. Wedl *, L. Schmieder, C. Hein, F. Winter

Institute of Chemical, Environmental and Bioscience Engineering, Technische Universität Wien, Vienna, Austria

ARTICLE INFO

Keywords:
Energy storage
Waste energy
Renewable
TCES
Thermochemical energy storage
Suspension reactor
Continuously stirred tank reactor

ABSTRACT

Thermochemical energy storage can be used for heating applications, thereby helping to cut down on greenhouse gases from burning non-renewable fuels by offering a solution for seasonal heat storage. In the scope of the EU project RESTORE, a thermochemical energy storage is used to store low temperature waste heat and use it for district heating. This study presents the thermochemical energy storage as a new continuously stirred tank three-phase suspension reactor for storing heat from renewable sources or waste heat with almost no losses, in reaction. Therefore, the reactor was built of glass, where process parameters, such as the mean residence time, have been varied to obtain optimized results for thermochemical energy storage operating at the fixed temperature of 125 °C chosen due to project restrictions. The heat is used to dehydrate $CuSO_4{\cdot}5H_2O$ in the charging step and recovered by rehydrating $CuSO_4{\cdot}3H_2O$ or $CuSO_4{\cdot}H_2O$, respectively, while generating heat in the discharging step. Using a mixture of silicone and mineral oil to prevent foaming, conversion rates of over 94 % to $CuSO_4{\cdot}H_2O$ were reached in the charging step with the continuously stirred tank reactor, with 1 kW thermal power, 150 mm diameter and 900 mm height in continuous operation. In discharging operation, 100 % conversion from $CuSO_4{\cdot}H_2O$ to $CuSO_4{\cdot}5H_2O$ was measured. This paper lays the groundwork for a new technology for thermochemical heat storage in low temperature application.

1. Introduction

Heating globally corresponds to about 50 % of energy consumption, reflected in 40 % of global greenhouse gas emissions [1]. Heat energy from (seasonal) renewable sources and unused waste heat from industry offer great potential when stored over a long period, where the recoverable waste heat potential in European industry is estimated at 370 TWh per annum [2]. The theoretical waste heat potential is 918 TWh in Europe [3], where 51 % are low temperature waste heat below 100 °C. One way to store this heat with almost no losses is using reaction enthalpy from a reversible chemical reaction. Therefore, this study is part of the RESTORE project, where the low temperature waste heat should be recovered and stored using thermochemical energy storage.

In literature, several thermal energy storage (TES) systems are known besides thermochemical energy storage systems (TCES), like latent thermal energy storage (LTES), or sensible thermal energy storage (STES) [4]. Kalita et al. [5] classify sensible heat storages further into water-based, packed beds, aquifer and boreholes, the latent heat storages in active and passive and the thermochemical heat storages in absorption, adsorption, and chemical reaction systems. While physical systems like LTES and STES have high losses while storing energy [6,7], and are therefore capable of only short-term storage, chemical systems like TCES are capable of storing energy for a long period of time without significant losses [8]. Adapted from H. Bao et al. [9] and A. Solé et al. [10] a further classification of the thermochemical energy storage for charging temperatures up to 250 °C is shown in Fig. 1.

In Fig. 1, the different technologies for TCES are shown. While chemical reactions such as redox reaction, or carbonation need a charging temperature of at least 434 °C for redox reaction, and 310 °C for carbonation [9], hydration can be archived at 200 °C [11] and, the chemical absorption requires a charging temperature lower than 100 °C [9]. The metal halides as part of the chemisorption have a wide charging temperature range from −50 °C to 350 °C while the salt hydrates used for chemical adsorption presented by H. Bao et al. [9] need a charging temperature between 50 °C and 186 °C. The TCM used for this study of thermochemical energy storage is described as chemical reaction of salt hydrates with a temperature range of interest set to 50 °C to 250 °C, where the chemical principle is expressible as [12]

$$C + \Delta H_R \rightleftharpoons A + B \tag{1}$$

* Corresponding author.
E-mail addresses: guenter.wedl@tuwien.ac.at (G. Wedl), lena.schmieder@tuwien.ac.at (L. Schmieder), franz.winter@tuwien.ac.at (F. Winter).

https://doi.org/10.1016/j.applthermaleng.2024.123977
Received 25 December 2023; Received in revised form 4 June 2024; Accepted 16 July 2024
Available online 17 July 2024

Nomenclature

Δm_i	mass fraction (g/g)
T	temperature (°C)
Δh_R	reaction enthalpy (J/mol)
t	time (s)
ψ_G	gas volume in liquid (%)
x, y	stochiometric coefficients
A, B, C	chemical Species
τ	mean residence time (min)
V	volume flow (l/min)
V_R	reactor volume (l)
H:D	height to diameter ratio

Abbreviations

wt.%	weight percentage
TCES	thermochemical energy storage
TES	thermal energy storage
TCM	thermochemical material
STES	sensible thermal heat storage
LTES	latent thermal energy storage
CSTR	continuously stirred tank reactor
$H_2O_{(liq)}$	liquid water
$H_2O_{(gas)}$	water vapour
$CuSO_4{\cdot}5H_2O$	copper sulphate pentahydrate
$CuSO_4{\cdot}3H_2O$	copper sulphate trihydrate
$CuSO_4{\cdot}H_2O$	copper sulphate monohydrate
$CuSO_4$	copper sulphate anhydrate
N_2	Nitrogen
rpm	rotation per minute

In Eq. (1) *C* is a salt hydrate or acid as thermochemical material, while *A* and *B* are reactants, where *A* can be e.g., an anhydrate or *meta*-acid [11], and *B* is water. While *C* usually is a solid or a liquid, *A,* and *B* can be any phase.

The process of heat storage can generally be seen in three main phases [8]:

- Charging
- Storing
- Discharging

In the endothermic charging process, thermal energy is absorbed from an energy source, e.g., solar energy or waste energy from industry which is used for the dissociation of the thermochemical material *C*. The supplied energy is equivalent to the reaction enthalpy of formation. As a result, two species, *A* and *B* are formed that can be stored. The reaction during charging can be expressed as

$$C + \Delta H_R \longrightarrow A + B \tag{2}$$

After charging, components *A* and *B* can be separately stored with little or no energy loss and without degradation of the materials [8], depending on the storage conditions.

When *A* and *B* are combined, an exothermic discharging reaction will occur. The energy, which again is equivalent to the reaction enthalpy of formation, released from this reaction recovers the stored energy, while *C* is regenerated and can be reused. The reaction during discharging can be written as

$$A + B \longrightarrow C + \Delta H_R \tag{3}$$

For this process, the most common chemical reactors are classified by Clark [13] and Solé [10] into

- Fixed bed reactor (also called packed bed)
- Moving bed
- Fluidized bed

while Widhalm et al. [12] list the most common TCES technologies as follows:

- Fluidized bed reactor
- Free fall reactor
- Rotary kiln reactor
- Screw reactor

where only the fluidized bed reactor was evaluated for practical use by J. Widhalm [12], since moving bed reactors such as screw reactors and

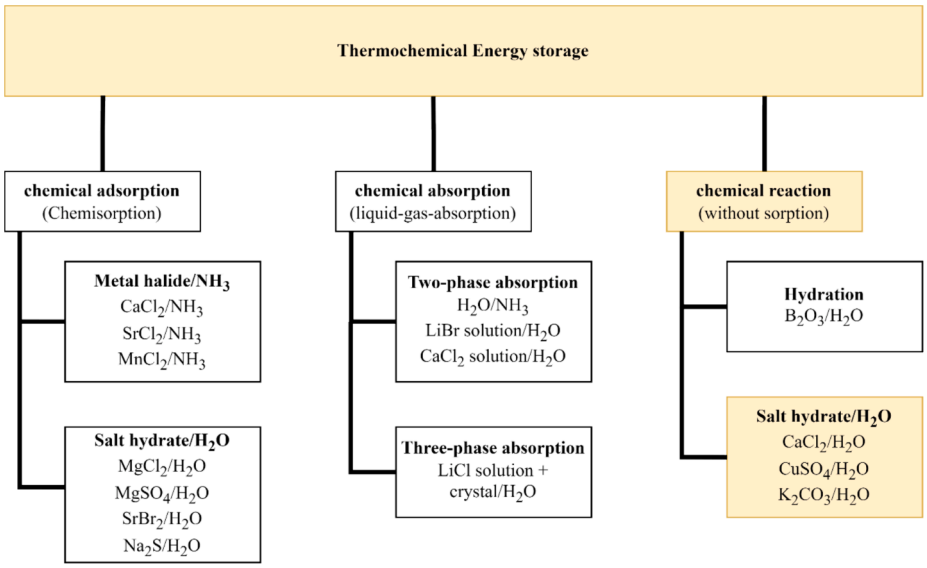

Fig. 1. Classification of thermochemical energy storage systems up to 250 °C adapted from Bao et al. [9] and A. Solé et al. [10].

rotary kiln reactors are complex to operate and seal because of the rotating mechanical system and the free fall reactor is not useable for TCES, due to its low residence time. Fluidized bed reactors have a high heat transfer coefficient, uniform particle mixing and good temperature control [13], but are limited by the particle size over the density difference between particle and fluidization gas [12], possible agglomeration, low conversion per unit volume, erosion of internal parts, higher energy requirements through pumping, and increased reactor vessel size [13]. Clark [13] on the other hand considers the fixed bed reactors as the most appropriate for TCES application due to the solid–gas states but sees major issues such as system heat capacity, heat losses and heat and mass transfer as well as large temperature gradients throughout the bed as restriction in its application.

To gain better heat and mass transfer and a homogeneous mixing of solids and liquids Garofalo et al. [14] proposed 2021 a novel approach using a suspension batch reactor with mineral oil as a suspension medium for TCES systems, having advantages over the aforementioned chemical reactors in their specific fields, which also resulted in a patent [15].

In this study, the first continuous stirred tank three-phase suspension reactor for TCES will be presented.

For choosing a suitable TCM for this continuous stirred tank three-phase suspension reactor, the following main criteria can be determined [10,16]:

- High volumetric heat storage density
- Non-toxicity
- Low price

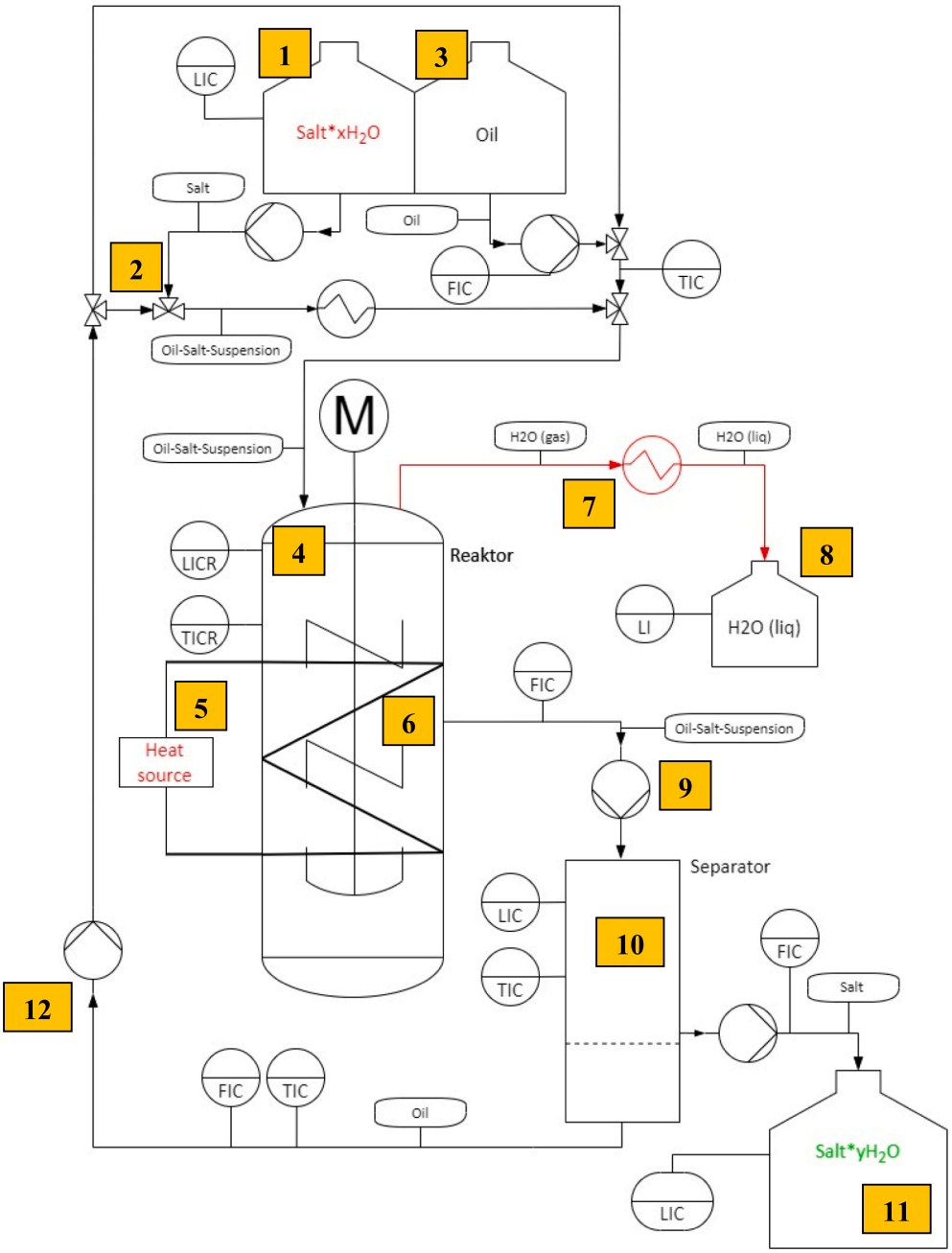

Fig. 2. Principle of charging reaction in a continuous stirred tank reactor.

P. Donkers gives an overview over 563 different the salt hydrates for heat storage [17], which had been narrowed down by A. Palacios [18] to $CaSO_4$, $MgSO_4$ and $CuSO_4$. From these candidates $CuSO_4$ was chosen as TCM not only because it changes its color [19] when it changes its hydration state, which allows to follow the reaction by sight, but also by its high energy density and suitable temperature range for charging and discharging. The theoretical energy density from $CuSO_4{\cdot}H_2O$ to $CuSO_4{\cdot}5H_2O$ was calculated to 2.073 GJ/m^3 with gaseous water as reactant, using the HSC database [20]. $CuSO_4{\cdot}5H_2O$ has been tested in batch experiments for agglomeration, cycle stability, charging and discharging temperature, where the optimal charging temperature was found to be 125 °C for conversion into $CuSO_4{\cdot}H_2O$ before the use in the CSTR.

The aim of this study is to build a lab-scaled prototype of a continuous stirred tank reactor for TCES as core technology in the EU Horizon project RESTORE where a reversable organic Rankine cycle should be combined with the TCES in a low temperature range, suitable for district heating.

2. Materials and methods

In the newly developed continuously stirred tank reactor (CSTR) salt-hydrates are used as thermochemical material. Therefore, Eq. (1) can be rewritten into

$$Salt{\cdot}xH_2O + Heat \rightleftharpoons Salt{\cdot}yH_2O + (x-y)H_2O \quad (4)$$

Since not every salt-hydrate would be reduced to salt-anhydrate, due e.g., to a too-low-temperature heat source, or the last reaction step needs

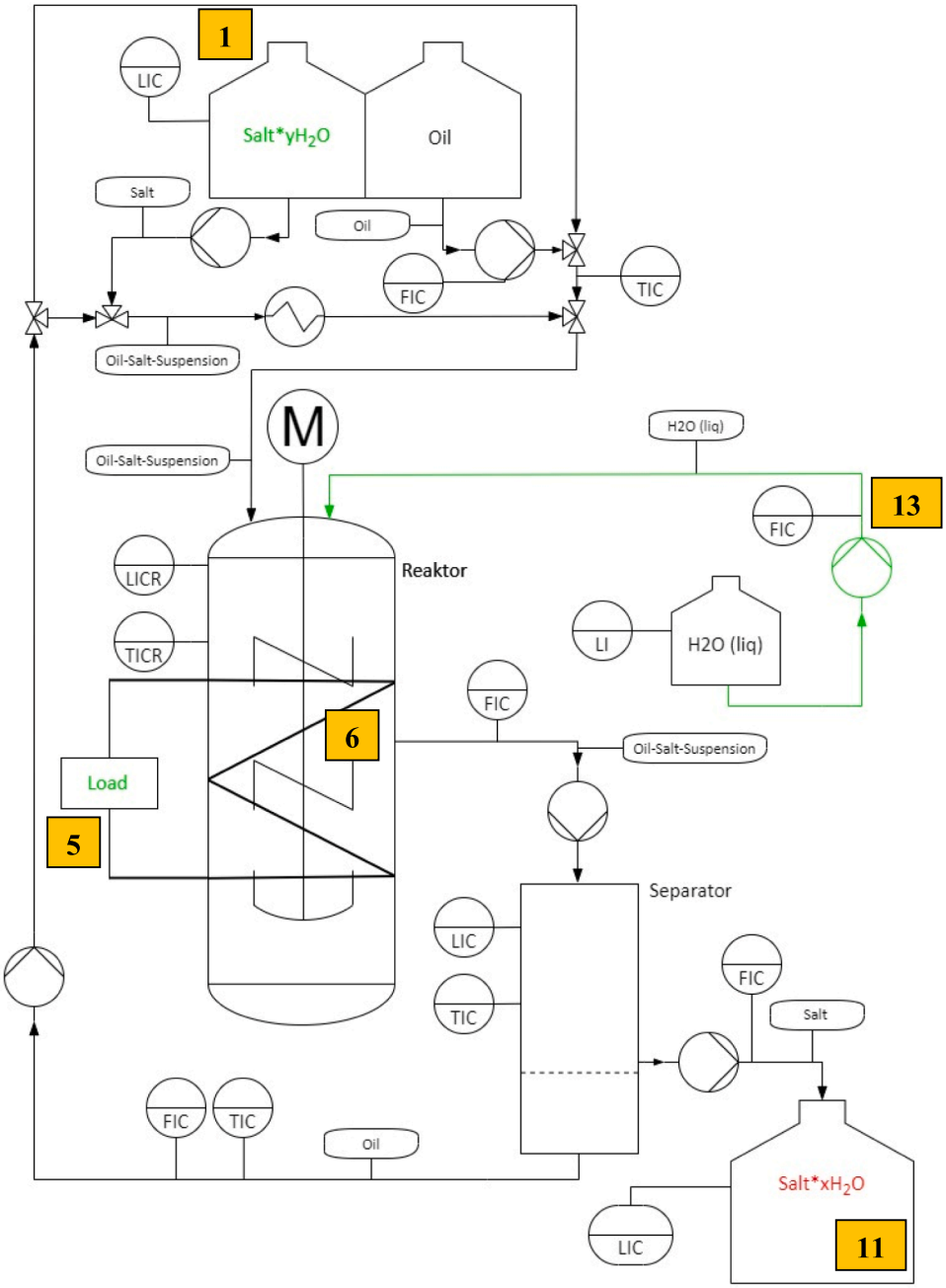

Fig. 3. Principle of discharging reaction.

exponentially more energy than the other steps, or in the last step, an unwanted reaction like agglomeration would occur, in the product part of the Eq. (4) the salt still contains yH$_2$O crystal water, where y can also be zero.

The principle of the charging reaction in the continuous stirred tank suspension reactor can be seen in Fig. 2.

The salt hydrate is transported from the salt tank (1) to the mixer (2) where the salt is preheated with recirculated hot oil (12). The suspension is diluted with recirculated hot oil and oil from the oil tank (3), if necessary, and transported into the stirred tank reactor (4). With the individual adjustable mass flow of recirculated oil, salt from the salt tank (1), and oil from the oil tank (3), the solid–liquid ratio of the suspension can be controlled. Therefore, the level change of the feeding salt tank (1), the oil flow of the recirculated oil, and the mass flow of the fresh oil are monitored and used to control the pumps. In the reactor (4), heat is supplied from an external heat source (5) through a heat exchanger (6), which provides the necessary energy for the reaction. The state of the reaction can be monitored by the temperature in the reactor. The gaseous water is condensed (7) after leaving the reactor and collected in the water tank (8). The reacted suspension is pumped (9) into the separator (10), which is built as a suction filtration. The filter cake is transported in the salt tank (11) while the filtrated oil is recirculated (12). The salt feed from the salt tank (1) into the mixer, the mixing (2) and the feed into the reactor (4) as well as the extraction of the reacted salt from the separator (10) are done with screw conveyors.

The extracted salt is covered in oil for storage, which prevents humidity from the air to discharge the charged salt and therefore, prolongs the storage period in contrast to uncovered salt.

The principle of the discharging reaction in the continuous stirred tank suspension reactor can be seen in Fig. 3.

The discharging process is done similarly to the charging process; therefore, only the differences will be explained. As opposed to the charging process, the material which is fed into the reactor is now the salt in its lower hydrate or anhydrate form from the salt tank (1). For the reaction to take place, water has to be added stoichiometrically with a pump (13), which can be done if the mass flow of the salt and its conversion state is known. While discharging, the reaction enthalpy, in form of heat, can be used through the heat exchanger (6), where now a load (5) instead of a heat source is operated which holds the reactor at a constant temperature. The salt hydrate is then extracted into the salt tank (11) while the oil is recirculated.

Different salts have been tested as thermochemical material (TCM) in the reactor, such as calcium chloride dihydrate [21] or copper sulphate pentahydrate ($CuSO_4{\cdot}5H_2O$). In this paper $CuSO_4{\cdot}5H_2O$ will be shortly described as TCM, since copper sulphate changes its color depending on its hydrated state from deep blue to white, which allows to visibly follow the reaction in a first approach. Since the RESTORE projects aims for thermochemical energy storage below 150 °C, $CuSO_4{\cdot}5H_2O$ will be only dehydrated to $CuSO_4{\cdot}H_2O$ and not to $CuSO_4$. Copper sulphate follows in this case a two-step reaction for dehydration [22]

$$CuSO_4{\cdot}5H_2O + Heat \rightleftharpoons CuSO_4{\cdot}3H_2O + 2H_2O \tag{5}$$

$$CuSO_4{\cdot}3H_2O + Heat \rightleftharpoons CuSO_4{\cdot}H_2O + 2H_2O \tag{6}$$

The rehydration is usually a one-step reaction, where only $CuSO_4{\cdot}5H_2O$ is formed

$$CuSO_4{\cdot}H_2O + 4H_2O \rightleftharpoons CuSO_4{\cdot}5H_2O + Heat \tag{7}$$

$$CuSO_4{\cdot}3H_2O + 2H_2O \rightleftharpoons CuSO_4{\cdot}5H_2O + Heat \tag{8}$$

The stored energy Q is the reaction enthalpy ΔH_R ($Heat$) of the used thermochemical material, depending on its conversion state. For storing the energy, heat, which cannot be stored in the TCM occurs in form of sensible heat, which is needed to transfer the heat via the oil to the TCM. The sensible heat can be expressed through [23]

$$Q = \int_{T_1}^{T_2} m c_p dT \tag{9}$$

In Eq. (9) m, c_p, and T represents the mass, specific heat capacity, and temperature of the oil, while T_1 and T_2 indicate the beginning and end of the heat transfer process [23].

Fig. 4 shows the built continuous stirred tank suspension reactor, which is a narrow stirred tank reactor with an inner height-to-width ratio H:D (Height to Diameter) of 90:15 (in cm) with a stirred volume of 14 l and a total volume of 22 l, including all pipes and the separator. The heat transfer for heating or cooling is done by an inner heating/cooling coil, within the range of 1 kW thermal power. The first prototype reactor is built from used glass parts where the reactor and separator use a flat flange system and the pipes use a ball flange system. The small pipes have an inner diameter of 25 mm, while the bigger pipes have an inner diameter of 50 mm. Glass was chosen as material for the prototype, since it has the notable advantage of being transparent so the reaction and flow regimes can be monitored; furthermore, thermal losses are not a priority for the small experiments.

The salt from the feeding system (1) is transported into the reactor

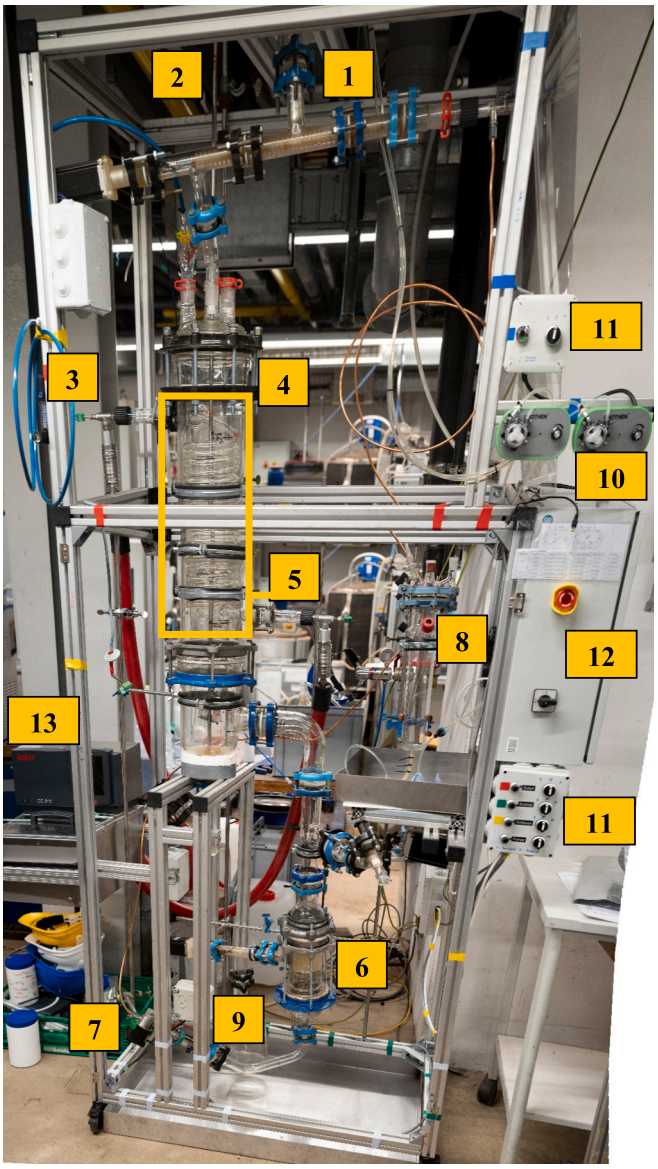

Fig. 4. Continuous stirred tank reactor.

(4), wherein the reaction zone (5) the charging or discharging reaction occurs. The heating or cooling in the reaction zone is supplied by the Huber CC 315 thermostat (13). For charging reactions, N_2 can be supplied for better vapor transport where the flow can be adjusted with a Brooks rotameter (3). The water is condensed and stored in a water tank (8). In the reaction zone (5), two propeller stirrers for a vertical flow and an anchor stirrer at the bottom for a horizontal flow were installed on one axis (2). This axis, until the lower end of the reaction zone (5), is hollow so that water for the discharging reaction can be injected through the axis into the reaction zone via Grothen G728-2 peristaltic pumps (10). Therefore, the rotary union SMC MQR1-M5 is used to decouple the water pipes from the stirrer axis. The salt-oil suspension is separated in the separator (6) via suction filtration where the salt is transported to a storage tank with a screw conveyor (9). The hot oil is recirculated by a VIPTech Mini 1200 Brushless geared pump (7) and used to preheat the salt in the feeding system. The screw conveyors, the geared pump, and an optional rotary valve can be controlled with hand potentiometers on control boxes (11), where also the direction of rotation for the screw conveyor and the optional rotary valve can be switched. The speed of the peristaltic pumps and the rotations per minute (rpm) of the stirrer are controlled directly at the devices. The power supply, the emergency stop switch, the on/off switch as well as a data logger Ketotek Smart Energy Monitor for electric consumption, and a data logger NI cDAQ-9171 for temperature measurement are installed into the switch cabinet (12). The temperature is measured by type K temperature sensors, where one sensor each is installed at the beginning and the end of the heat-transfer coil, respectively, and four temperature sensors are installed inside the reactor at different heights (each at the top of the reactor, top of the reaction zone, bottom of the reaction zone and bottom of the reactor). Additionally, one temperature sensor is installed at the hot oil inlet of the feeding system, one at the pump outlet, and one in the water tank.

Fig. 5 shows the feeding system of the prototype continuous stirred tank suspension reactor.

In Fig. 5 (a) the salt (not shown here) from the salt tank (1) is transported with a screw conveyor (2) to the screw conveyor (3) where the salt is mixed with the recirculated hot oil and thereby preheated. The oil is fed to the screw conveyor (3) over the recirculation pipe (4). While suspending the salt in the oil the suspension is transported into the reactor (5). The salt tank is shown from the side in Fig. 5 (b) where the hoses (7) in Fig. 5 (b) are used to transport water into the hollow stirrer shaft (8) during rehydration reaction. The 3D printed screw conveyors are driven by two stepping motors ACT 23HS2442B (6) with the motor driver ACT DM545. The control of the motor driver is done with an Arduino Nano Every, where a hand potentiometer is used for the signal manipulation, but automatic control with a computer can be implemented. The velocity of each screw conveyor and the geared pump for the oil recirculation can be adjusted separately.

For separation, two different concepts were tested, suction filtration and sedimentation. Fig. 6 shows the installed suction filtration separator (a) and the inner separation unit (b).

The mesh support structure (1) and the screw conveyor (2) are 3D printed with Formlabs High-Temperature V2 resin. The filter mesh (3) has a mesh width of 400 μm and is fixated on the support structure with M2 screws (6). The mesh support structure is glued into the glass cylinder with silicon (4), which is also used for sealing all gaps between the filtration unit and the glass cylinder. To hold the inner separation unit in place while gluing, a coarse metal mesh (5) is used.

Fig. 7 shows the sedimentation tank with the reactor (a), the emptied sedimentation tank (b) and the deflector and inlet of the sedimentation tank (c).

The suspension is inserted in the sedimentation tank in the upper third of the tank through an internal pipe (2) coming from the top of the tank (1). The sedimented salt is extracted from the bottom of the tank through a rotary valve (3), while the oil leaves the sedimentation tank from the top (4). A deflector (5) prevents a short circuit of the suspension from the inlet to the outlet of the sedimentation tank. The sedimentation tank increased the total volume of the reactor by 7l.

Fig. 8 shows the used stirrer with its counter bearing (a) and the water outlet in the reaction zone (b).

The stirrer consists of three stirrer blades, where the two upper stirrer blades are a pitched blade stirrer (1) and a propeller stirrer (2) for axial stirring in the reaction zone, while the lower stirrer blade (3) is a paddle stirrer to prevent sedimentation on the bottom of the reactor and helping the particles in suspension to exit the reactor. The stirrer shaft consists of a hollow upper part and a massive lower part which are connected through a small piece of a steel pipe (5). For rehydration, water can be pumped through the holes (6) in the hollow shaft.

Fig. 9 shows the installed sparger for N_2 (Nitrogen) bubbling.

While charging, foaming occurred, which is a dispersion of gas (water vapor from the reaction) in a liquid (mineral oil) with a gas volume of $\psi_G > 52\%$ [24] in a high energetic state due its extraordinarily large interface between the gaseous and liquid phases [25]. To prevent foam, the surface tension can be minimized [26], or the bubble diameter can be maximized to destabilize the foam [27]. Therefore, a

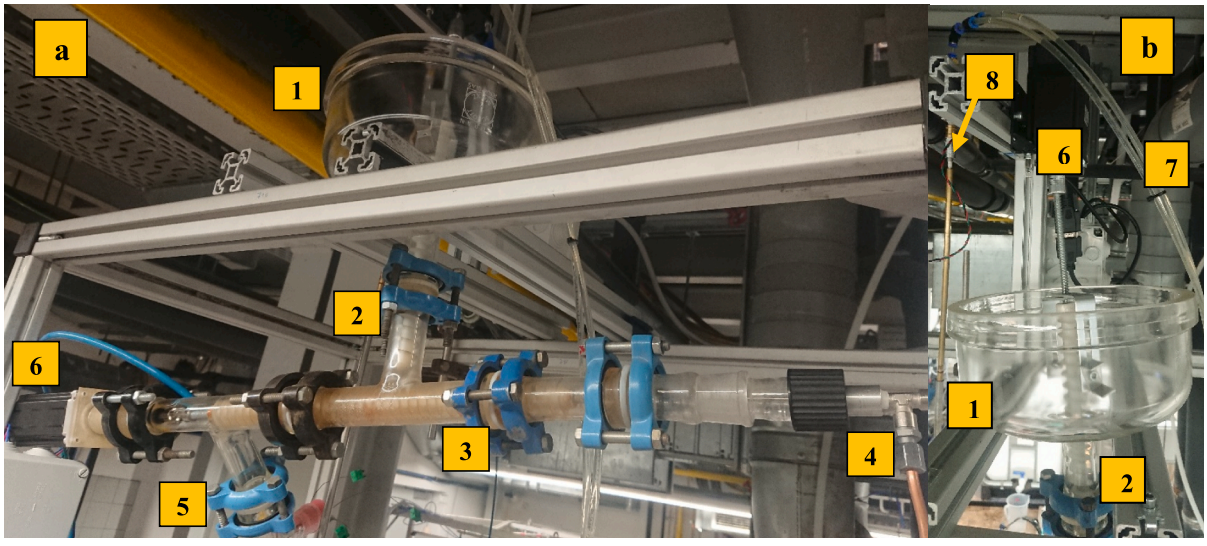

Fig. 5. The feeding system consists of a salt tank (1), a screw conveyor (2) for transporting the salt to the mixer, and a screw conveyor (3) for mixing the salt with hot oil (4) and transporting the suspension into the reactor (5) (a) and a detail view on the salt tank (b).

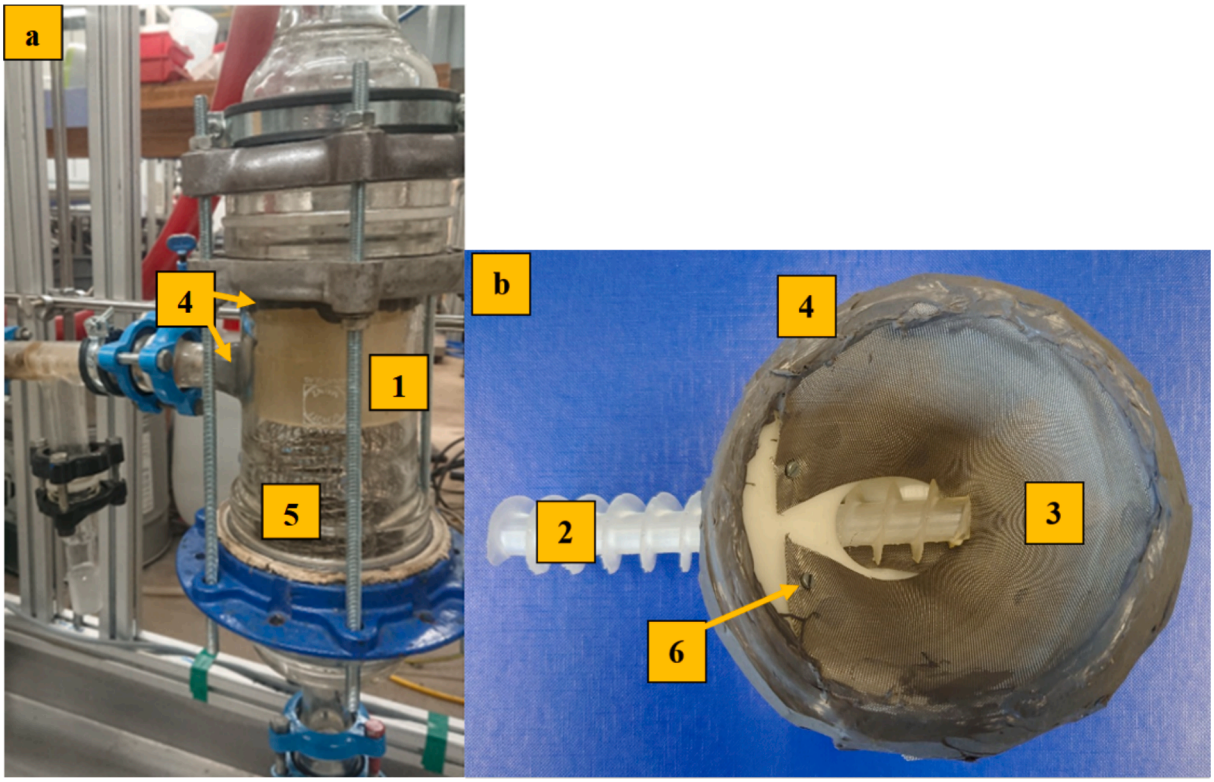

Fig. 6. Installed separator (a), and support structure with filter mesh and screw conveyor (b).

sparger has been installed to generate N_2 bubbles which coalescence with the water vapor.

Depending on the separation method, two different extraction methods for the separated salt have been used. From the suction filtration, a 3D-printed screw conveyor transported the salt from the filter into a storage vessel, while for the sedimentation tank, a home-made steel rotary valve is used to convey the salt from the bottom of the sedimentation tank into the storage bin.

As for the Methodology, the conversion rate of the thermochemical material was determined with a PANalytical X'Pert Pro diffractometer in Bragg-Brentano geometry with Cu $K_{\alpha1,2}$ radiation, a BBHD mirror filter, and a X'Celerator line-detector. The measure range was from 5° to 70° in 2θ degrees. The estimated maximum error margin of the measurement was ±2.7 wt% of the main phase but typically ±2 wt% of the main phase. For analysis of the diffractogram, HighScore Plus for element determination and Topas for the composition from PANnalytical and PaNdata was used, respectively, using the Rietveld method from 15° to 70° in 2θ degrees. To analyse the samples, 20 g of each taken sample had been vacuum filtered on a glass frit and rinsed twice with petroleum ether. From each conducted experiment 5 samples were taken directly form the rotary valve outlet, one after each other in an interval of 10 min.

The temperature was measured by type K class II temperature sensors using a data logger NI cDAQ-9171 with the NI 9211 module and LabView.

The mass flow of the recirculating oil was determined by the flow sensor YF-S201 and an Arduino to calculate the flow using the following core code:

```
flowrate = (count * 2.25);
flowrate = flowrate * 60;
flowrate = flowrate / 1000;
```

In the first line the counted pulses (count) over the measure time (1 s) are multiplied by the volume of one segment (2.25 mL) of the rotary wheel of the sensor and assigned to the variable "flowrate". In the second line, the flowrate is converted in ml/min and in the last line in l/min.

For the measurement of the water flow, the sensor ifm electronic SM4000 was used.

The input mass flow was determined by the velocity of the screw conveyer. Therefore, tests had been conducted where the conveyed volume at different velocities for the dry mass fraction and the oil-salt suspension typical in the salt tank was measured gravimetrically. The estimated error is ±10 % due to the manual sample taking.

The nitrogen flow was measured using one MR3A12 and two MR3A15 rotameters from Key Instruments, where all of them have an uncertainty of ±4 %.

Table 1 gives a summary of the main technical parameters of the test rig which could be adjusted, how they were measured and the estimated uncertainty of the measured results.

The Experimental procedure is similar but still different for the charging and discharging reaction. Therefore, the operation of the reactor in charging and discharging mode will be explained separately.

For the charging reaction the reactor was at first filled with the mineral/silicone oil mixture. Thereafter, the thermostat and the stirrer of the reactor were switched on. To avoid agglomeration, the stirrer speed was set to 500 rotations per minute (rpm). While the reactor was heating up, the pump for oil recirculation was switched on and the $CuSO_4{\cdot}5H_2O$ was filled into the salt tank with some mineral/silicone oil mixture, and the nitrogen flow for the sparger was started. After the reactor reached operation temperature, the recirculation flow was adjusted and the screw conveyers for transporting the salt into the reactor were started. When the reaction took place, the temperature had to be monitored closely and the heat output of the thermostat was adjusted, if necessary. Depending on the mean residence time, after the mean residence time plus 2–3 min to amass enough particles over the rotary valve, the rotary valve was started to extract the converted salt. The extracted oil-covered salt was collected in a bucket. Every 10 min a sample was taken directly from the outlet of the rotary valve. For long

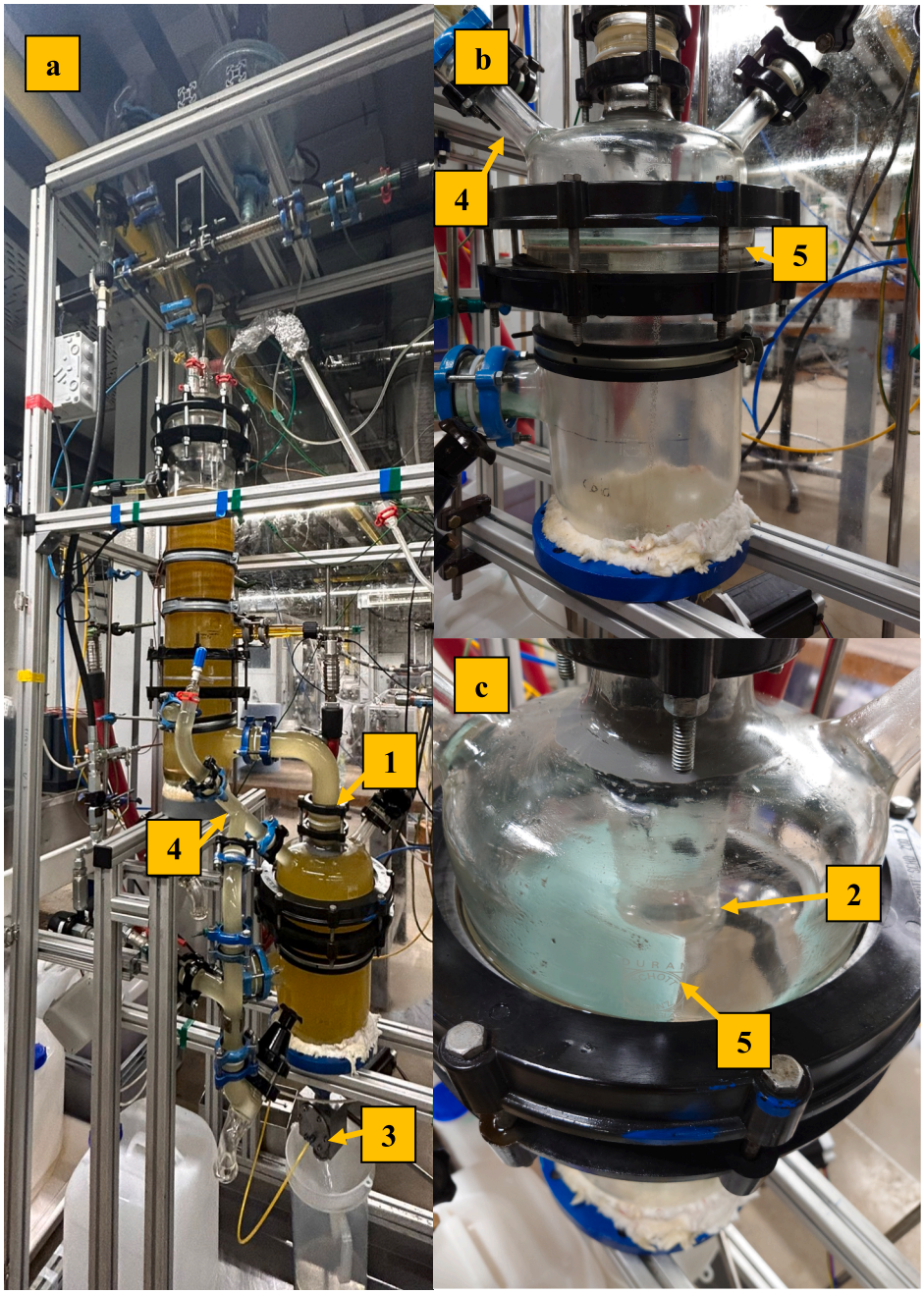

Fig. 7. Sedimentation Tank.

time experiments, the salt and oil in the salt tank had to be replenished. After the salt was used up, the reactor was still operated for at least two times the mean residence to make sure that all particles had been transported out of the reactor and sedimented. In a last step the thermostat was shut down and the pumps, stirrer, and rotary valve stopped. To get rid of possible agglomerations in the dead volume of the reactor, the oil was flushed out of the reactor while still hot. Table 2 summarizes the experiments presented here.

For charging reaction, 5 experiments are presented in this study, where the mean residence time was varied through the recirculation mass flow. The goal of these experiments was to find the optimum operation parameters in scope of the project for maximum output. Therefore, the extracted salt was analysed using XRD and then used for the discharging reaction.

For the discharging reaction the reactor was filled up with the mineral/silicone oil mixture. The silicone oil is not needed for the discharging reaction but since the mixture was available from the charging experiments, it was used. The stirrer was again set to 500 rpm to avoid agglomeration, but the thermostat was now used for cooling with a temperature of 40 °C. The nitrogen flow for the sparger was started for better mixing and the salt tank was filled with the $CuSO_4{\cdot}3H_2O/CuSO_4{\cdot}H_2O$ mixture from the previous charging experiment. The water tank was filled with enough water for the reaction and the water flow in the reactor was adjusted according to the calculations of the needed water for reaction plus 10 % excess water. After the recirculation flow was started and adjusted, the screw conveyer of the salt tank and the water pump were switched on. After the mean residence time plus 2–3 min to amass enough particles over the rotary valve, the rotary valve was started to extract the converted salt. Again, the extracted oil covered salt was collected in a bucket. Every 10 min a sample was taken directly from the outlet of the rotary valve. After the salt was used up, the reactor was still operated for at least two times the

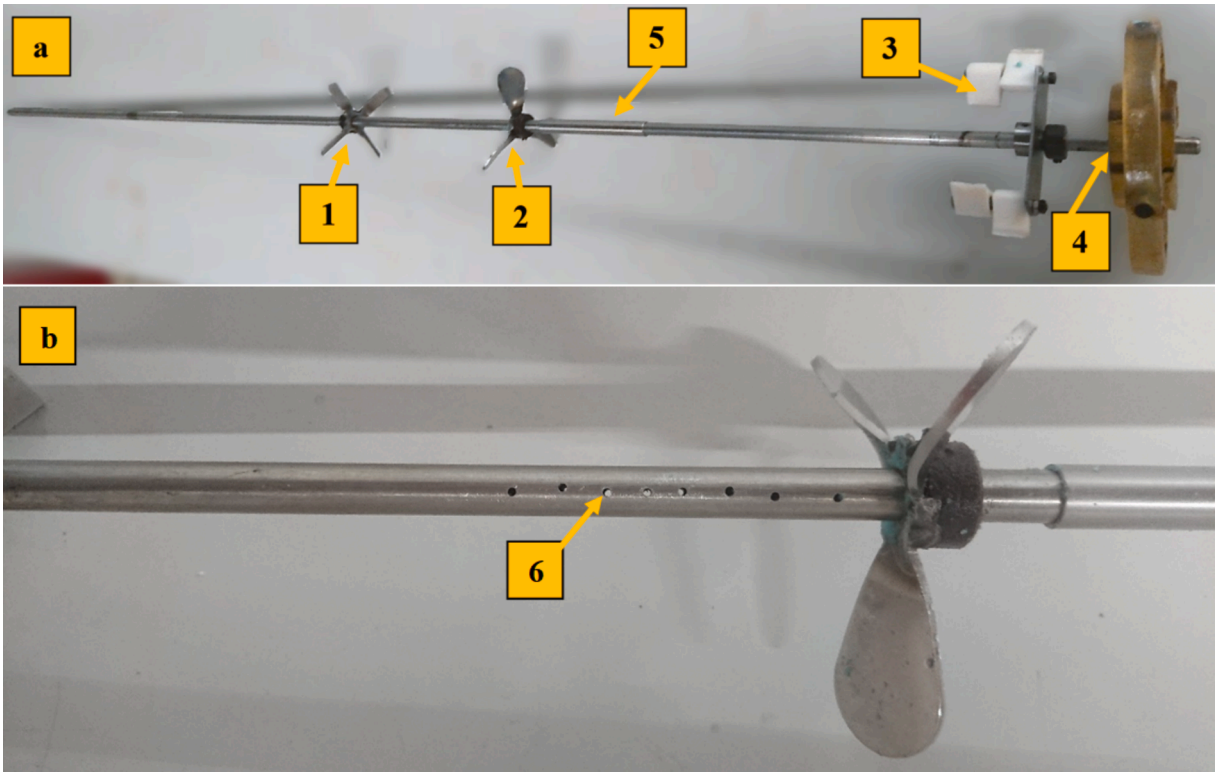

Fig. 8. Stirrer (a) and water outlet from hollow shaft (b).

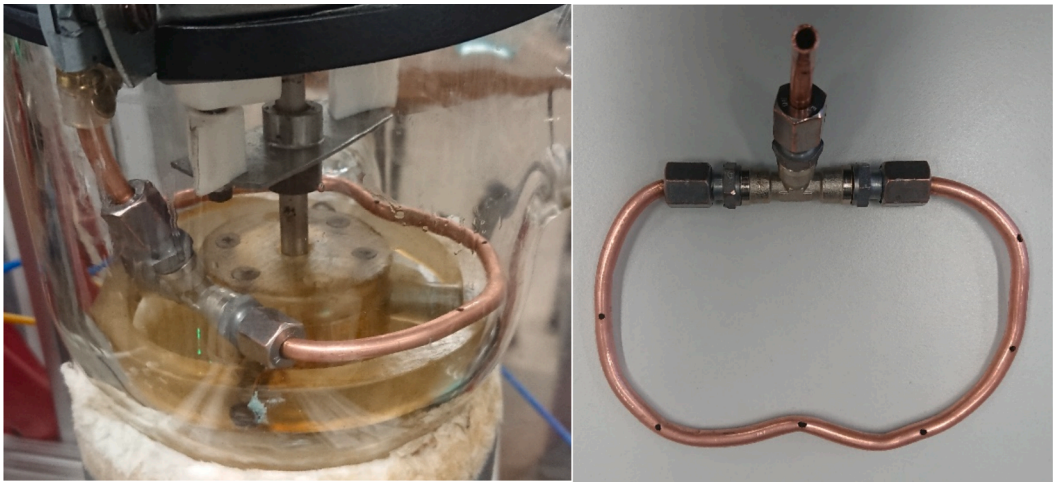

Fig. 9. Sparger in reactor (a) and sparger (b).

Table 1
Summary of the main parameters and their measurement uncertainty.

Parameter	*Measurement device*	*Uncertainty*
Recirculation oil flow	Flow meter YF-S201	± 10 %
Water flow	Flow meter SM4000	± 2 %
Salt input mass flow	Gravimetrically determined	± 10 %
Temperature	Typ K class II temperature sensors	± 2.5 °C
N_2 flow	Rotameter MR3A12 and MR3A15	± 4 %
Conversion	XRD	± 2.5 %

mean residence to make sure that all particles had been transported out of the reactor and sedimented. For the reactor shut down, the thermostat, the pumps, stirrer, and rotary valve were stopped. In a last step, the reactor was cleaned while the oil was still warm. Table 3 summarizes the experiments presented here.

For discharging, two experiments with different mean residence time have been conducted and the extracted salt was analysed using XRD, with the goal to find the optimized operation parameters.

3. Results and discussion

The mean residence time τ is controlled by the pumping power and is calculated through [28]

$$\tau = \frac{V_R}{\dot{V}} \tag{10}$$

where V_R is the reactor volume and V is the volume flow of the reactor, while the reactor volume is kept constant. The mean residence time

Table 2
Experiments conducted for charging reaction.

Experiment	*Recirculation mass flow*	*N_2 flow*	*Input mass flow*	*Temperature*
1	3 l/min	Head volume: 1.5 l/min	8.3 g/min	125 °C
2	2 l/min	Head volume: 1.5 l/min	8.3 g/min	125 °C
3	1.5 l/min	Head volume: 1.5 l/min	8.3 g/min	125 °C
4	1 l/min	Head volume: 1.5 l/min	8.3 g/min	125 °C
5	1 l/min	Head volume: 0.5 l/min Sparger: 6 l/min	8.3 g/min	125 °C

Table 3
Experiments conducted for discharging reaction.

Experiment	*Recirculation mass flow*	*Water flow*	*Input mass flow*	*Temperature*
1	2.5 l/min	11.7 ml/min	41 g/min	40 °C
2	4.5 l/min	11.7 ml/min	41 g/min	40 °C

gives a rough indication of the time a particle spent in the reactor, since only the outflow of the oil is measured.

The kinetics were determined in pre-experiments, which have shown that the dehydration form $CuSO_4{\cdot}5H_2O$ to $CuSO_4{\cdot}H_2O$ takes place in around 15 min at 125 °C, while the rehydration from $CuSO_4{\cdot}H_2O$ to $CuSO_4{\cdot}5H_2O$ only needs around 3 min starting at room temperature. Therefore, the outflow of the reactor can be calculated to 1 l/min for dehydration (charging) and 4.7 l/min for rehydration (discharging), using Equation (10).

The conversion rate was determined with a PANalytical X'Pert XRD diffractometer. The diffractogram after processing with Topas is depicted in Fig. 10, where the calculated fit is overlapping the diffractogram. Fig. 11 shows the results for dehydration of 5 different experiments, where in the first 4 experiments the mean residence time was varied from 4.7 min to 14 min by constant temperature and in the last experiment the 4th experiment with a mean residence time of 14 min was repeated but with the additional sparger installed. All presented experiments were conducted with the sedimentation tank used for separation. The progression of the conversion until the reactor reaches a steady state is shown in Fig. 12.

In Fig. 10 the XRD result after calculating the weight percentage of the found compounds with the Rietveld method using the Topas program is shown. The compounds have been found with the Highscore plus program, using the "profile and peak" search method. The error for the diffractogram in Fig. 10 has an error of ±2.5 % of the main phase Poitevenite ($CuSO_4{\cdot}H_2O$) and ±2.5 % of the second phase Bonattite ($CuSO_4{\cdot}3H_2O$).

In Fig. 11 the conversion of $CuSO_4{\cdot}5H_2O$ is shown for different mean residence times, where the lower part of the bar represents $CuSO_4{\cdot}H_2O$, the middle part of the bar $CuSO_4{\cdot}3H_2O$ and the top part the unconverted $CuSO_4{\cdot}5H_2O$. While the conversion to the desired $CuSO_4{\cdot}H_2O$ is only slightly over 50 % for short residence times, the overall conversion of $CuSO_4{\cdot}5H_2O$ to a mixture of $CuSO_4{\cdot}3H_2O$ and $CuSO_4{\cdot}H_2O$ is nearly 100 % for all used mean residence times. With a mean residence time $\tau = 14$ min, a conversion to $CuSO_4{\cdot}H_2O$ of 84 % was measured. With the sparger a conversion of 94.7 % could be achieved since, through the counter current of the gas from the sparger in the reactor, the particle

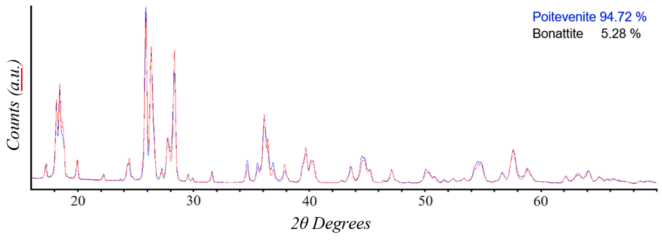

Fig. 10. XRD measurement of the conversion of $CuSO_4{\cdot}5H_2O$ to lower hydrates.

mean residence time had been prolonged. The maximum error which occurred in the measurements was ±2.7 % of the main phase, but the mean error was ±2.5 % of the main phase.

In Fig. 12 it can be seen that the conversion of all samples to $CuSO_4{\cdot}H_2O$ increases in the beginning up to its final conversion of the continuous operation (sample 5) is reached at the given conditions. This can be explained with the temperature profile, shown in Fig. 13, which is exemplary for the conducted experiments.

As soon as the reactor has reached operation temperature, $CuSO_4{\cdot}5H_2O$ was added (1), which resulted in a temperature drop because of insufficient heat transfer through the glass heating coils of the reactor. After the heat transport into the reactor was adjusted (2), the temperature started rising again, leading to a better conversion of the material.

In the preheating phase, at first only the stirred reactor was heated and then the pump was switched on, causing a sharp rise of the preheater and pump curves (3). When the rotary valve was operated in a way that not only salt but also oil was transported outside the sedimentation tank, air was transported into the sedimentation tank, causing a drop of temperature in the preheater and pump curves (4).

Table 4 shows the results of rehydration of one experiment with a mean residence time of $\tau = 3.11$ min and $\tau = 5.6$ min, respectively.

For the experiment, converted $CuSO_4{\cdot}5H_2O$, consisting of a mixture of $CuSO_4{\cdot}H2O$ and $CuSO_4{\cdot}3H2O$, from an experiment described above was used, and the water needed was calculated according to the XRD results plus 10 % excess water. For separation, the sedimentation tank was used. From the experiment, 2 samples were taken in an interval of 10 min. The nonconverted material in the fourth line of Table 1 most likely comes from residues from former experiments in the reactor. The reactor was actively cooled through the thermostat with tap water through the experiment. With the longest mean residence time of 5.6 min, the rehydration is very fast in the suspension reactor, contrary to the study of Ferchaud et al. [29].

For each presented dehydration experiment, 0.5 kg of $CuSO_4{\cdot}5H_2O$ had been transported into the reactor over the period of 1 h. This results in a mass flow of 0.12 kg/15 min, which is the mean mass of solids in the reactor for an outflow of 1 l/min. Therefore, the dehydration with $\tau = 14$ min was performed with 1 wt% mass fraction in the reactor.

For the rehydration experiment, 1 kg of the $CuSO_4{\cdot}H_2O$/$CuSO_4{\cdot}3H_2O$ mix had been used over the period of 20 min, which results in 4.5 wt% mass fractions in the reactor.

The mass fractions of TCM in the reactor is now too low, since a lot of energy would be converted into sensible heat instead of being stored as reaction enthalpy. Therefore, further experiments for process intensification will be conducted, but first simulations showed that with the reactor in the current form, the main limiting factor will not only be the heat transfer from the heat source into the reactor, but the currently used heat source itself, which provides 3.5 kW heating power at maximum, sufficient for only 4.5 wt% mass fractions of TCM.

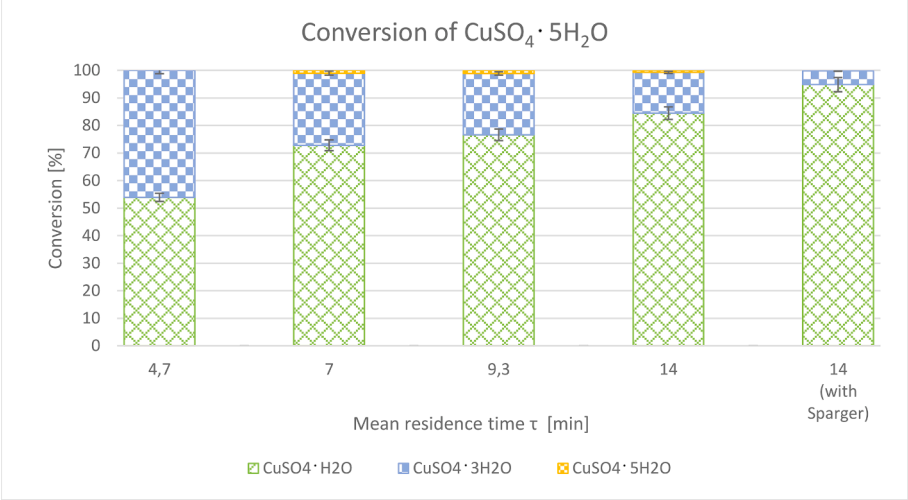

Fig. 11. Conversion of $CuSO_4 \cdot 5H_2O$ to lower hydrates in relation to the mean residence time.

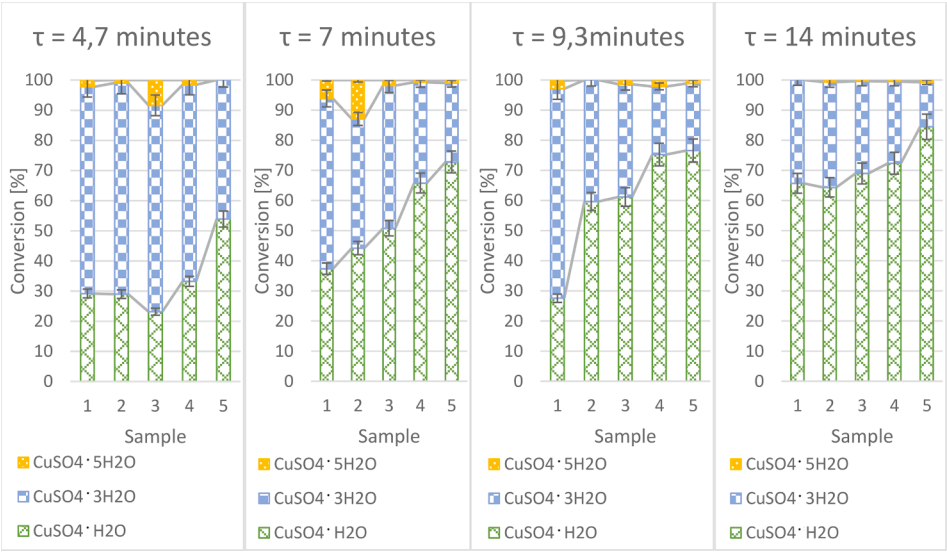

Fig. 12. Progression of conversion in the startup phase.

The limiting factor of the suction filtration is the mesh size. If the mesh is too fine, the resistance for the oil flow will be high up to the point where the oil flow might be blocked. If the mesh is too coarse, fine particles would not be held back which results in loss of material, accumulation of dead material and potentially problems in the pump.

The suction filtration worked well for the first batch of $CuSO_4 \cdot 5H_2O$, which was a leftover of 900 g found in the laboratory. The newly ordered $CuSO_4 \cdot 5H_2O$ from the same company had a different particles size distribution which was shifted to smaller main fractions, as shown in Fig. 14, and was therefore not suited for suction filtration anymore.

Fig. 14 (a) shows the particle size distribution of the found leftover $CuSO_4 \cdot 5H_2O$ with a main fraction of 600 μm particles, while (b) shows the newly ordered $CuSO_4 \cdot 5H_2O$ with a main fraction of 315 μm particles.

For sedimentation, the height of the tank and the mean residence time in the tank are one of the main characteristics. Therefore, sieve analyses have been conducted not only on $CuSO_4 \cdot 5H_2O$ but also on the $CuSO_4 \cdot 3H_2O/CuSO_4 \cdot H_2O$ mixes gained from dehydration experiments, which are shown in Fig. 15.

Comparing Fig. 15 with Fig. 14 (b), the mass fractions above 400 μm disappear and, since $CuSO_4 \cdot 5H_2O$ particles break down to smaller particles during dehydration [22]. Also, Donkers et al. [30] observed the breakdown of the copper particles during dehydration, using a fixed bed reactor, but contrary to that study, no decrease of the stability of the dehydration/rehydration of $CuSO_4$ could be observed in the continuously stirred suspension reactor.

To determine the minimum height of the sedimentation tank, the terminal velocity of the smallest particle must be found. Therefore, the sedimentation experiments have been conducted, where from each fraction from the sieve analysis some particles were sedimented in a glass cylinder with tempered oil at 120 °C and markings each 5 cm. The results are shown in Table 5.

With the measured terminal velocity of the slowest sinking particles of $0.64 \cdot 10^{-3}$ m/s in the hot oil and the mean residence time of 14 min of the sedimentation tank, the minimum height of the tank can be calculated to 58 cm.

During dehydration, severe foaming occurred with mineral oil. Since foaming is dependent on the surface area, temperature, and surface tension [31], the lowering of the surface tension can avoid foaming. Since silicone oil is a widely used foam inhibitor, a mixture of silicone oil and mineral oil was used in a first approach. With a ratio of 15 wt% silicone oil in mineral oil, foaming could be successfully prevented. As mentioned before, bigger bubble sizes can destabilize foam, which is

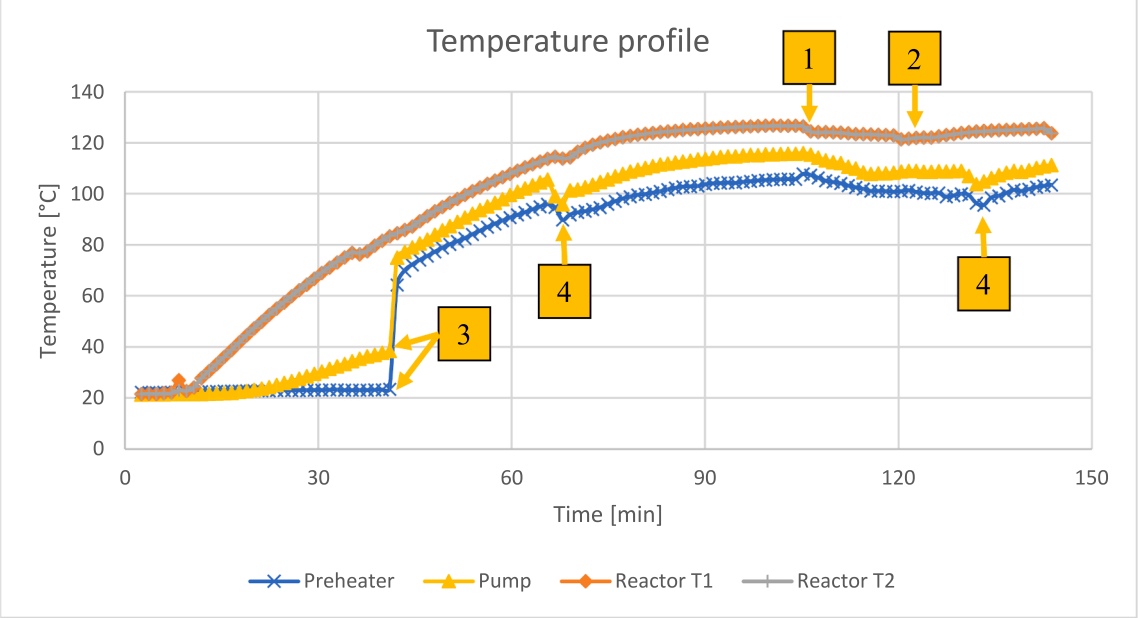

Fig. 13. Temperature profile with 1.5 l/min out flow of the reactor, where T1 is in the upper part of the reactor and T2 is the sensor in the bottom part of the reactor.

Table 4
Conversion of $CuSO_4{\cdot}3H_2O$ and $CuSO_4{\cdot}H_2O$ to $CuSO_4{\cdot}5H_2O$.

Flowrate	*$CuSO_4{\cdot}H_2O$*	*$CuSO_4{\cdot}3H_2O$*	*$CuSO_4{\cdot}5H_2O$*	*τ*	*T*
(l/min)	(%)	(%)	(%)	(min)	(°C)
2.5	0	0	100	5.6	40
4.5	0.7	0	99.3	3.11	40

why a sparger for N_2 was installed at the bottom of the reactor for bubble coalescence of the N_2 bubbles with the emerging vapor. With the sparger and a N_2 flow of 6 l/min the silicone oil ratio could be lowered to 7 wt% silicone oil in mineral oil.

4. Conclusion

The newly developed continuously stirred tank three-phase suspension reactor was successfully tested with copper sulphate in a mineral-/silicone-oil mixture with different mean residence times, ranging from 4.7 min to 14 min at 125 °C as a core technology for the thermochemical energy storage in the scope of the RESTORE project. The residence time of the particles in the reactor can be varied through the oil flow of the oil recirculation. The optimized parameters for the chemical charging reaction were found with a mean residence time of 14 min and a sparger using 6 l/min N_2 flow, resulting in a conversion rate to the desired $CuSO_4{\cdot}H_2O$ copper sulphate of 94.8 %, where $CuSO_4{\cdot}5H_2O$ was fully converted. Rehydration or discharging was performed at 3.1- and 5.6-minutes mean residence time, respectively and reached 100 % conversion to $CuSO_4{\cdot}5H_2O$. The waste heat needed for the reaction was successfully simulated with a thermal oil through an inner heat exchanger coil for heating and cooling within the range of 1 kW thermal power. Due to the breakdown of $CuSO_4$ particles during dehydration and the excessively small particles of some available $CuSO_4{\cdot}5H_2O$ salts, initially the suction filtration was not working and had to be replaced by a sedimentation tank. Foaming occurred during dehydration of $CuSO_4{\cdot}5H_2O$, which could be prevented by using a mixture of 15 wt% silicone oil in mineral oil without sparger and 7 wt% silicone oil in mineral oil using a N_2 sparger. The newly developed three-phase suspension reactor shows promising results in charging and discharging of salt – oil systems for thermochemical heat storage and will be used in a

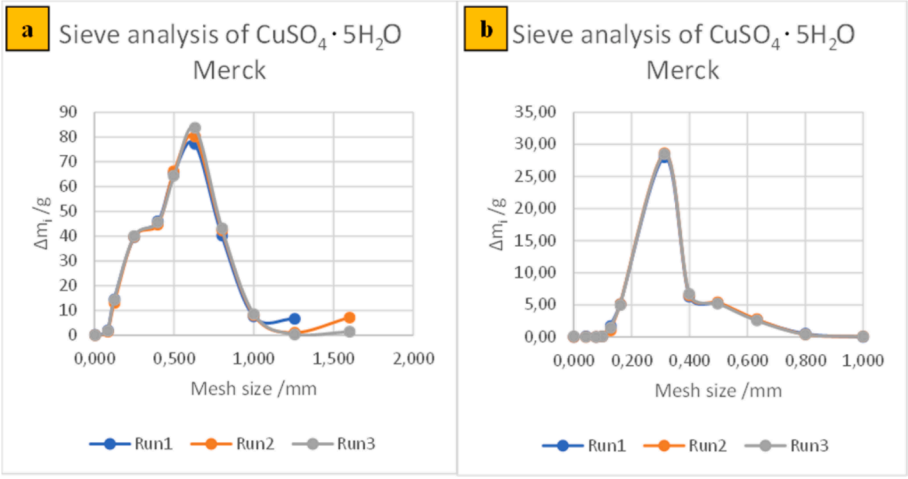

Fig. 14. Comparison of particle size distribution of old and newly ordered $CuSO_4{\cdot}5H_2O$.

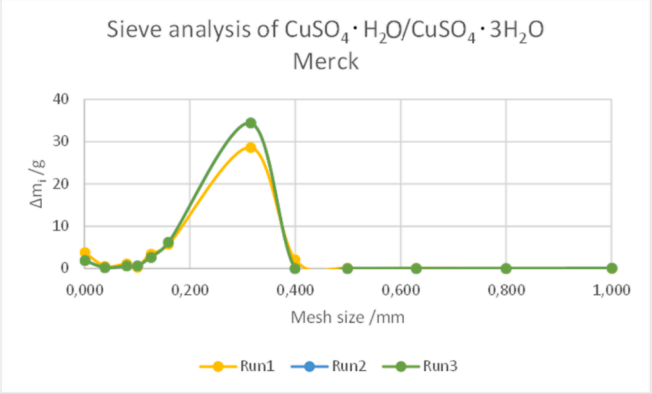

Fig. 15. Particle size distribution of $CuSO_4{\cdot}3H_2O/CuSO_4{\cdot}H_2O$.

Table 5
Terminal velocity for each fraction of the sieve analysis.

Species	*sieve − class*	*Ø (mm)*	v_t *(m/s)*	m/τ ($\tau = 14$ min)
$CuSO_4{\cdot}5H_2O$	Ø > 100 µm	0.10	0.00064	0.58
$CuSO_4{\cdot}5H_2O$	Ø > 125 µm	0.125	0.00101	0.91
$CuSO_4{\cdot}5H_2O$	Ø > 160 µm	0.16	0.00165	1.49
$CuSO_4{\cdot}5H_2O$	Ø > 315 µm	0.315	0.00641	5.77
$CuSO_4{\cdot}3H_2O$/ $CuSO_4{\cdot}H_2O$	Ø > 125 µm	0.125	0.00125	1.13
$CuSO_4{\cdot}3H_2O$/ $CuSO_4{\cdot}H_2O$	Ø > 160 µm	0.16	0.00206	1.85
$CuSO_4{\cdot}3H_2O$/ $CuSO_4{\cdot}H_2O$	Ø > 315 µm	0.315	0.00799	7.19
$CuSO_4{\cdot}3H_2O$/ $CuSO_4{\cdot}H_2O$	Ø > 400 µm	0.40	0.01288	11.59

further study where $CuSO_4$ will be analyzed for its full potential as TCM, with experiments on long-term operation, process intensification and energy balances. Also, tests of other thermochemical materials up to 250 °C are planned. In the scope of the project, a scaled-up version of the presented reactor will be built.

Declaration of competing interest

The authors declare that they have no known competing financial interests or personal relationships that could have appeared to influence the work reported in this paper.

Data availability

Data will be made available on request.

Acknowledgment

The author thanks the European Union's Horizon 2020 research and innovation program, RESTORE, under grant agreement No 101036766 for funding. The authors acknowledge TU Wien Bibliothek for financial support through its Open Access Funding Program. Also the author wants to thank Jakob Smith for XRD meassurements and proof reading.

References

[1] A. Vannoni, A. Sorce, A. Traverso, A. Fausto Massardo, Techno-economic optimization of high-temperature heat pumps for waste heat recovery, Energy Convers. Manag. 290 (2023), https://doi.org/10.1016/j.enconman.2023.117194.
[2] S.O. Oyedepo, B.A. Fakeye, Waste heat recovery technologies: pathway to sustainable energy development, J. Therm. Eng. 7 (1) (2021) 324–348.
[3] G. Bianchi, et al., Estimating the waste heat recovery in the European Union Industry, Energy Ecol Environ 4 (5) (2019) 211–221, https://doi.org/10.1007/s40974-019-00132-7.
[4] X. Chen, Z. Zhang, C. Qi, X. Ling, H. Peng, State of the art on the high-temperature thermochemical energy storage systems, Energy Convers Manag 177 (2018) 792–815, https://doi.org/10.1016/j.enconman.2018.10.011.
[5] P. Kalita, D. Kashyap, U. Bordoloi, Thermal energy storage systems for cooling and heating applications, in: Photoconductivity and Photoconductive Materials: Fundamentals Energy Storage, Wiley, 2021, pp. 149–199, https://doi.org/10.1002/9781119555599.ch5.
[6] L. G. Socaciu, Leonardo Electronic Journal of Practices and Technologies Seasonal Sensible Thermal Energy Storage Solutions, 2011, [Online]. <http://lejpt.academicdirect.org>.
[7] H. Jouhara, A. Żabnieńska-Góra, N. Khordehgah, D. Ahmad, T. Lipinski, Latent thermal energy storage technologies and applications: a review, Int. J. Thermofluids 5–6 (2020), https://doi.org/10.1016/j.ijft.2020.100039.
[8] A.H. Abedin, M.A. Rosen, A critical review of thermochemical energy storage systems, Open Renew. Energy J. 4 (2011) 42–46.
[9] H. Bao, Z. Ma, Thermochemical energy storage, in: Storing Energy: with Special Reference to Renewable Energy Sources, Elsevier, 2022, pp. 651–683, https://doi.org/10.1016/B978-0-12-824510-1.00028-3.
[10] A. Solé, I. Martorell, L.F. Cabeza, State of the art on gas-solid thermochemical energy storage systems and reactors for building applications, Renew. Sustain. Energy Rev. 47 (2015) 386–398, https://doi.org/10.1016/j.rser.2015.03.077.
[11] C. Huber, et al., Boric acid: a high potential candidate for thermochemical energy storage, Energies (Basel) 12 (6) (2019), https://doi.org/10.3390/en12061086.
[12] J. Widhalm, T. Fellner, M. Deutsch, A. Werner, F. Winter, Thermochemical energy storage as a way to increase the sustainability of energy generation, in; Asian Conference on Sustainability, Energy and the Environment, Kobe, 2015.
[13] R.J. Clark, A. Mehrabadi, M. Farid, State of the art on salt hydrate thermochemical energy storage systems for use in building applications, J. Energy Storage 27 (2020), https://doi.org/10.1016/j.est.2019.101145.
[14] L. Garofalo, F.V. Vitiello, F. Montagnaro, H. Bürgmayr, F. Winter, Salt Hydrates for thermochemical storage of solar energy: modeling the case study of calcium oxalate monohydrate dehydration/rehydration under suspension reactor conditions, Ind. Eng. Chem. Res. 60 (30) (2021) 11357–11372, https://doi.org/10.1021/acs.iecr.1c01220.
[15] F. Winter, J. Tomasich, H. Bürgemayer, K.H. Steinkellner, Thermochemical energy storage device, WO2022159998 A1, 2022.
[16] K.E. N'Tsoukpoe, T. Schmidt, H.U. Rammelberg, B.A. Watts, W.K.L. Ruck, A systematic multi-step screening of numerous salt hydrates for low temperature thermochemical energy storage, Appl. Energy 124 (2014) 1–16, https://doi.org/10.1016/j.apenergy.2014.02.053.
[17] P.A.J. Donkers, L.C. Sögütoglu, H.P. Huinink, H.R. Fischer, O.C.G. Adan, A review of salt hydrates for seasonal heat storage in domestic applications, Appl. Energy 199 (2017) 45–68, https://doi.org/10.1016/j.apenergy.2017.04.080.
[18] A. Palacios, M.E. Navarro, C. Barreneche, Y. Ding, Experimental validation of thermochemical water-sorption materials for thermal energy storage: building application, Sustain. Mater. Technol. 38 (2023), https://doi.org/10.1016/j.susmat.2023.e00702.
[19] M.A. Ibrahim, R.T. Boeré, The copper sulfate hydration cycle. Crystal structures of CuSO4 (Chalcocyanite), CuSO4·H2O (Poitevinite), CuSO4·3H2O (Bonattite) and CuSO4·5H2O (Chalcanthite) at low temperature using non-spherical atomic scattering factors, New J. Chem. 46 (12) (2022) 5479–5488, https://doi.org/10.1039/d2nj00169a.
[20] Outotec, HSC Chemistry, 2007.
[21] L. Schmieder, Calcium chloride dihydrate as a promising system for seasonal heat storage in a suspension reactor, Appl. Therm. Eng. under review (2024).
[22] L. Cheng, et al., Thermal analysis and decomposition kinetics of the dehydration of copper sulfate pentahydrate, J. Therm. Anal. Calorim. 135 (5) (2019) 2697–2703, https://doi.org/10.1007/s10973-018-7595-y.
[23] W. Hua, H. Yan, X. Zhang, X. Xu, L. Zhang, Y. Shi, Review of salt hydrates-based thermochemical adsorption thermal storage technologies, J Energy Storage 56 (2022), https://doi.org/10.1016/j.est.2022.106158.
[24] M.H. Pahl, D. Franke, Foam and foam breaking - a review, in: Chemie-Ingenieur-Technik, vol. 67, no. 3, Wiley-VCH Verlag, 1995, pp. 300–312, https://doi.org/10.1002/cite.330670306.
[25] A. Frank, W. Scholz, Defoamers in the coatings industry, Add. Plast. Paints Chimia 56(5) (2002) 177–183, [Online]. Available: www.byk-chemie.com.
[26] C. Fehn, "Untersuchungen zur Stabilität von Tensidschäumen," Bayreuth , 2006. Accessed: Mar. 19, 2024. [Online]. Available: https://epub.uni-bayreuth.de/id/eprint/759.
[27] Y. Zhang, R.J. Fruehan, Effect of the bubble size and chemical reactions on slag foaming, Metall. Mater. Trans. B 26B (1995) 803–812.
[28] O. Levenspiel, The mean and variance of a tracer curve, Fluid Mech. Appl. 96 (2012) 5–10, https://doi.org/10.1007/978-1-4419-8074-8_2.
[29] C. J. Ferchaud, H. A. Zondag, R. De Boer, C. J. Ferchaud, H. A. Zondag, R. De Boer, Material research on salt hydrates for seasonal heat storage application in a residential environment, in: Proceedings International Symposium on Innovative Materials for Processes in Energy System (Impress 2013), Fukuoka, Japan, 2013. [Online]. Available: www.tue.nl/taverne.
[30] P.A.J. Donkers, L. Pel, O.C.G. Adan, Experimental studies for the cyclability of salt hydrates for thermochemical heat storage, J. Energy Storage 5 (2016) 25–32, https://doi.org/10.1016/j.est.2015.11.005.
[31] D. Beneventi, B. Carre, A. Gandini, Role of surfactant structure on surface and foaming properties, Colloids Surf. A Physicochem. Eng. Asp 189 (2001) 65–73. www.elsevier.nl/locate/colsurfa.